DOI: 10.1534/genetics.105.044222

Identification of a Rat Model for Usher Syndrome Type 1B by *N*-Ethyl-*N*-nitrosourea Mutagenesis-Driven Forward Genetics

Bart M. G. Smits,* Theo A. Peters,† Joram D. Mul,* Huib J. Croes,‡ Jack A. M. Fransen,‡ Andy J. Beynon,† Victor Guryev,* Ronald H. A. Plasterk* and Edwin Cuppen*,[1]

**Hubrecht Laboratory, Centre for Biomedical Genetics, 3584 CT Utrecht, The Netherlands,* †*Department of Otorhinolaryngology and* ‡*Department of Cell Biology, Radboud University, 6500 HB Nijmegen, The Netherlands*

Manuscript received April 11, 2005
Accepted for publication May 16, 2005

ABSTRACT

The rat is the most extensively studied model organism and is broadly used in biomedical research. Current rat disease models are selected from existing strains and their number is thereby limited by the degree of naturally occurring variation or spontaneous mutations. We have used ENU mutagenesis to increase genetic variation in laboratory rats and identified a recessive mutant, named tornado, showing aberrant circling behavior, hyperactivity, and stereotypic head shaking. More detailed analysis revealed profound deafness due to disorganization and degeneration of the organ of Corti that already manifests at the onset of hearing. We set up a single nucleotide polymorphism (SNP)-based mapping strategy to identify the affected gene, revealing strong linkage to the central region of chromosome 1. Candidate gene resequencing identified a point mutation that introduces a premature stopcodon in *Myo7a*. Mutations in human *MYO7A* result in Usher syndrome type 1B, a severe autosomal inherited recessive disease that involves deafness and vestibular dysfunction. Here, we present the first characterized rat model for this disease. In addition, we demonstrate proof of principle for the generation and cloning of human disease models in rat using ENU mutagenesis, providing good perspectives for systematic phenotypic screens in the rat.

THE rat is the most frequently used organism in a wide spectrum of biomedical studies, *e.g.*, physiological and nutritional studies, and drug development. Recently, the rat became the third mammal for which the complete genome was sequenced (Gibbs *et al.* 2004). Nevertheless, mammalian geneticists favor the mouse above the rat as a model organism (Gibbs *et al.* 2004), which is mainly due to the differences in the availability of tools for the manipulation of their genomes. Reverse genetic or knockout technology to disrupt the expression of a gene is well established for the mouse (reviewed in Bockamp *et al.* 2002; van der Weyden *et al.* 2002), but has become available only very recently for the rat by means of *N*-ethyl-*N*-nitrosourea (ENU) mutagenesis (Zan *et al.* 2003; Smits *et al.* 2004). In addition, forward genetic approaches have been successfully employed in the mouse for several decades, primarily by employing ENU mutagenesis for the efficient generation of novel models (reviewed in O'Brien and Frankel 2004).

Several large-scale mouse forward genetic screens for ENU-induced mutations have been initiated (reviewed in Keays and Nolan 2003). The screens are phenotype driven, employing appropriate assays on mutant animals to identify phenotypes that resemble aspects of human disease. The resulting models are expected to contribute substantially to the understanding of genetic diseases (Cox and Brown 2003).

For the rat, however, the >200 existing models (Hedrich 2000; Jacob and Kwitek 2002) are primarily selected from existing laboratory strains and their number and nature is therefore limited by the degree of naturally occurring variation or the occurrence of spontaneous novel mutations. Nevertheless, important rat models exist for common human diseases (Greenhouse *et al.* 1990), including hypertension, diabetes, cancer, and many others (Jacob *et al.* 1992; Shepel *et al.* 1998; Rapp 2000). ENU mutagenesis would have the potential to induce a major increase in the number of rat phenotypes and models, as it has done for the mouse (Brown and Nolan 1998; Brown and Balling 2001).

While ENU mutagenesis conditions have recently been established for the rat (Zan *et al.* 2003; Smits *et al.* 2004), additional bottlenecks for efficient forward genetics are still present. First, establishment of comprehensive and efficient high-throughput screening setups will be challenging, although the rat has already been used for decades as the primary model organism in, for example, behavioral neurobiology, hypertension, and diabetes research. As a result, extensively validated assays are available and provide a solid basis for the development of a rat screening protocol. Second, cloning of the causal

[1]*Corresponding author:* Functional Genomics Group, Hubrecht Laboratory, Uppsalalaan 8, 3584 CT Utrecht, The Netherlands.
E-mail: ecuppen@niob.knaw.nl

mutations underlying aberrant phenotypes depends on the availability of efficient genetic mapping and cloning tools. Currently, the availability of genetic markers to scan the rat genome for linkage to traits of interest is limited. Although a large collection of microsatellite markers has been genotyped in variety of strains and successfully used for mapping and cloning purposes (Chwalisz *et al.* 2003; Kuramoto *et al.* 2004), the application of the more versatile single nucleotide polymorphism (SNP) markers in the rat is still in its infancy. Large repositories of rat SNPs and candidate SNPs became available recently (Guryev *et al.* 2004; Zimdahl *et al.* 2004), but information on SNP distribution in different strains is still mostly lacking.

In this study, we describe the identification and characterization of the first autosomal recessive mutant rat strain from an ENU mutagenesis-driven study. Animals from this strain display locomotory hyperactivity, circling behavior, and stereotypic head shaking. More detailed characterization reveals that these animals are deaf due to progressive degeneration of the organ of Corti. For mapping and cloning purposes, we designed and tested a genome-wide SNP-based mapping panel for Wistar *vs.* Brown Norway (BN)-based crosses, which allowed us to pinpoint the mutation to a chromosomal subregion containing a limited number of strong candidate genes. With the subsequent identification of a premature stopcodon in one of these genes, *Myo7a*, we established a rat model for the human Usher syndrome type 1B (USH1B) and provided proof of concept for ENU-driven forward genetics in the rat.

MATERIALS AND METHODS

Animals, ENU mutagenesis, and crosses: Male Wistar founder rats (WIS/Crl) were mutagenized using ENU (Sigma, St. Louis). Mutagenesis was carried out as described (Smits *et al.* 2004). Briefly, intraperitonial (i.p.) injections of ENU were given in three weekly doses. One male received 3 × 40 mg/kg body weight, and three males received 3 × 20 mg/kg body weight. The injected animals were mated with untreated females (WIS/Crl) to establish a F_1 population, which was primarily used for a large-scale reverse genetics screen described elsewhere (Smits *et al.* 2004). Eight F_1 males and eight F_1 females were selected from this population and used to set up crosses, preventing brother-sister matings. Next, F_2 progeny from these crosses was used in 18 different brother-sister matings to breed induced mutations to homozygosity, resulting in a single nest with the aberrant tornado (*tnd*) phenotype.

For the mapping cross, two male tornado animals ware mated with four Brown Norway females (BN/Crl). From the F_1 generation, 10 males and 10 females were intercrossed to restore the tornado phenotype.

DNA isolation, PCR, and sequencing: For genotyping, animals were tail clipped under isoflurane anesthetics. Lysis on tail clips was done overnight at 55° in 400 μl lysis buffer, containing 100 mm Tris (pH 8.5), 200 mm of NaCl, 0.2% of SDS, 5 mm of EDTA, and 100 μg/ml of freshly added proteinase K. Samples were centrifuged for 15 min at 6000 × *g* and the supernatant was transferred to a fresh tube or plate. Genomic DNA was isolated by adding an equal amount of isopropanol, mixing, and subsequently centrifuging for 20 min at 6000 × *g*. Pellets were rinsed with 70% ethanol and dissolved in 400 μl H_2O. For PCR, 5 μl of a 50× dilution in water was used.

PCR was carried out using a touchdown thermocycling program (92° for 60 sec; 12 cycles of 92° for 20 sec, 65° for 20 sec with a decrement of 0.4° per cycle, 72° for 30 sec; followed by 20 cycles of 92° for 20 sec, 58° for 20 sec, and 72° for 30 sec; and 72° for 180 sec; GeneAmp9700, Applied Biosystems, Foster City, CA). PCR reaction mixes contained 5 μl genomic DNA, 0.2 μm forward primer, and 0.2 μm reverse primer, 200 μm of each dNTP, 25 mm tricine, 7.0% glycerol (w/v), 1.6% DMSO (w/v), 2 mm $MgCl_2$, 85 mm ammonium acetate, pH 8.7, and 0.2 units Taq polymerase in a total volume of 10 μl.

PCR products were diluted with 25 μl water and 1 μl was used as template for the sequencing reactions. Sequencing reactions, containing 0.25 μl BigDYE (v1.1; Applied Biosystems), 3.75 μl 2.5× dilution buffer (Applied Biosystems), and 0.4 μm gene-specific primer in a total volume of 10 μl, were performed using cycling conditions recommended by the manufacturer. Sequencing products were purified by ethanol precipitation in the presence of 40 mm sodium acetate and analyzed on a 96-capillary 3730XL DNA analyzer (Applied Biosystems). Sequences were analyzed for the presence of polymorphisms using polyphred (Nickerson *et al.* 1997). Primers for PCR amplification and sequencing were designed using the Ensembl genome database (http://www.ensembl.org) and a customized interface to Primer3 (Rozen and Skaletsky 2000).

Marker selection and testing for mapping: The panel of SNP markers, polymorphic between Brown Norway and Wistar rat strains, was extracted from the rat CASCAD candidate SNP database (Guryev *et al.* 2004; http://cascad.niob.knaw.nl) and verified in the six parents (two tornado males and four BN females) of the mapping cross by sequencing. The rat genome was virtually divided into 90 bins of similar size and the final SNP panel contained 84 verified SNPs representing 67 of these bins. The cross scheme already elucidated the autosomal recessive manner of inheritance for the mutation, so only markers on the autosomes were included to map the mutation. In total, the SNP distribution patterns for 67 mutant F_2 animals from the mapping cross were determined.

Scanning electron microscopy: Tornado animals ($Myo7a^{tnd\text{-}1Hubr}/Myo7a^{tnd\text{-}1Hubr}$) ($n = 7$) and phenotypically normal littermates ($Myo7a^{tnd\text{-}1Hubr}/+$ or $+/+$) ($n = 6$) of 6 days, 10 days, 20 days, and 13 weeks of age were examined. Rats were anesthetized by i.p. injection of Nembutal (60 mg/kg) and intracardially perfusion fixed with 2.5% glutaraldehyde in 0.1 m sodium-cacodylate buffer (pH 7.4). Inner ears were dissected and postfixed overnight in the same fixative. After fixation for 1 hr in 2% osmium tetroxide in 0.1 m sodium-cacodylate buffer, the specimens were dehydrated, critical point dried, and sputter coated with gold. Specimens were examined in a Jeol 6310 scanning electron microscope operating at 15 kV.

Light microscopy: Pigmented tornado animals ($Myo7a^{tnd\text{-}1Hubr}/Myo7a^{tnd\text{-}1Hubr}$) ($n = 2$), derived from a cross with Brown Norway animals and having a crossing over between the albino and tornado locus, and heterozygous, pigmented littermates ($Myo7a^{tnd\text{-}1Hubr}/+$) ($n = 2$) of 5 weeks of age were sacrificed. The eyes were dissected, fixed in buffered formalin overnight, and embedded in paraffin. Sections of 6 μm through the retina were prepared and stained with hematoxylin/eosin and examined using a Nikkon Eclipse 6600 light microscope.

Auditory brain-stem response measurements: Auditory brainstem response measurements (ABR) were performed in a soundproof room with low reverbation. Needle electrodes were placed on M1 and M2 (left and right mastoids) and referred to Cz (vertex) to record the auditory-evoked potentials. A ground

electrode was placed halfway on the tail of the rat. Interelectrode impedances were measured before and after each measurement (< 8 kohm). Click stimuli were presented in a soundfield by placing the loudspeakers 5 cm in front of each ear. The loudness levels at the position of the ear were measured and calibrated with a Bruel and Kjaer 2203 sound pressure level (SPL) meter. All thresholds were corrected afterward for the soundfield setup by −7 dB (SPL). Before the measurements were made, the rats were i.p. injected with Nimatek (100 mg/kg) anesthetics. A standard-evoked potential recording system (Synergy, Oxford Instruments) was used to present 100-μsec click stimuli with a fixed stimulation rate of 20 Hz. The analysis time was set at 15 msec from the onset of the click with a 1.5-msec prestimulus time to assess the baseline. The recorded EEG signals were high-pass filtered at 100 Hz and low-pass filtered at 3 kHz; an automatic artifact rejection and a 60-Hz notch-filter were used to obtain auditory brainstem responses from contra- and ipsilateral stimulation sites. The EEG signals were averaged for different stimulation levels according to standard audiometrical top-down procedures, starting at 90 dB (SPL), uncorrected for the soundfield. Peaks were identified according to the Jewett and Williston nomenclature (Jewett and Williston 1971). The auditory hearing threshold was defined as the level (in decibels) at which no reproducible responses were visually recognized in the responses obtained from the ipsilateral measured ear.

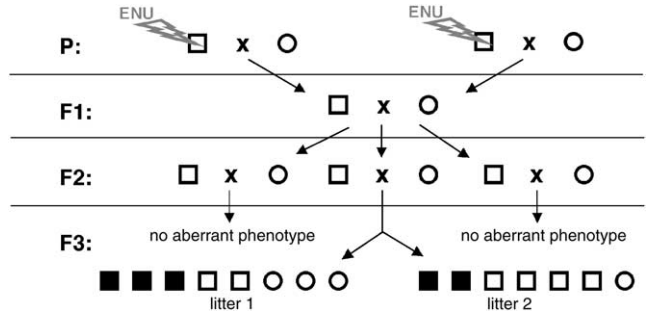

Figure 1.—Overview of the crosses that resulted in the identification of the tornado mutant. Four ENU mutagenized males were used to generate F_1 animals by crossing to untreated females. Sixteen breeding pairs were selected from this progeny to produce the F_2 generation. Brother-sister matings were set up for these animals to breed induced mutations to homozygosity to reveal potential recessive phenotypes. The figure represents all matings set up for a specific F_1 pair (the others did not result in any visually apparent aberrant phenotype). One of the three F_2 matings resulted in progeny with an aberrant phenotype that was named tornado. Genetic inheritance of the phenotype was confirmed in a second mating. Squares and circles represent males and females, respectively. Solid symbols indicate animals with the tornado phenotype.

RESULTS

Mutant phenotype: Rat models for human disease traditionally result from breeding of inbred strains that were specifically selected for naturally occurring aberrant traits (Hedrich 2000). We performed ENU mutagenesis in the rat (Smits *et al.* 2004) to increase the amount of genetic variation and conducted a small-scale screen for phenotypes caused by recessive mutations. Eight male and eight female F_1 animals derived from four ENU-treated founders were paired. Eighteen brother-sister matings for inbreeding-induced recessive mutations were set up from the resulting F_2 progeny. Animals were visually inspected for abnormalities and a single family was found in which three of the eight F_3 animals showed an aberrant, circling behavior (Figure 1; supplemental movie 1 at http://www.niob.knaw.nl/research pages/cuppen/publications/tornado) and were therefore named tornado. The mutant phenotype was confirmed to be inherited in an autosomal recessive manner by the second litter of that cross, producing two tornado animals among seven animals (Figure 1). Although initially only male animals with the tornado phenotype were identified in the F_3 generation, this should be considered a coincidence, since later matings using other animals also yielded female tornado animals in a normal Mendelian ratio (data not shown).

More detailed analysis of the tornado rats revealed, besides circling behavior, additional abnormalities. Deafness in the mutants was observed by a negative Preyer's reflex. Moreover, the mutant rats show locomotory hyperactivity, stereotypic head flicking, and vestibular dysfunction, which became evident in a swimming test (supplementary movie 2 at http://www.niob.knaw.nl/research pages/cuppen/publications/tornado). The complete phenotype strongly resembles the mouse shaker (Gibson *et al.* 1995; Wang *et al.* 1998), waltzer (Alagramam *et al.* 2001; Wilson *et al.* 2001), and whirler (Mburu *et al.* 2003) phenotypes for which a variety of underlying gene defects have been identified.

Mapping cross: To identify the genetic defect underlying the rat tornado phenotype, we set up a mapping cross using a Brown Norway background. The causal mutation was introduced in a Wistar background (Smits *et al.* 2004) and the Brown Norway strain is genetically the most distant compared to other commonly used laboratory rat strains (Canzian 1997; Thomas *et al.* 2003), making it the best strain for mapping purposes. Ten F_1 intercrosses were set up to restore the phenotype. In the first mating round, we obtained 117 F_2 animals, of which 34 displayed the tornado phenotype (not shown). Strikingly, all tornado animals were found to be albino, whereas none of the pigmented (brown or black) animals showed the phenotype, indicating linkage to the gene causing albinism in the Wistar strain (c), which is located on chromosome 1 (*Tyr*). Two albino animals did not show the tornado phenotype. Considering these animals to be crossing overs, the genetic distance between the mutation and *Tyr* was estimated to be ~3 cM.

Mapping the tornado mutation with the whole-genome SNP mapping panel: A genome-wide SNP mapping panel (Brown Norway *vs.* Wistar) was constructed to independently confirm linkage to chromosome 1. Therefore, the rat genome was distributed in 90 bins of equal size

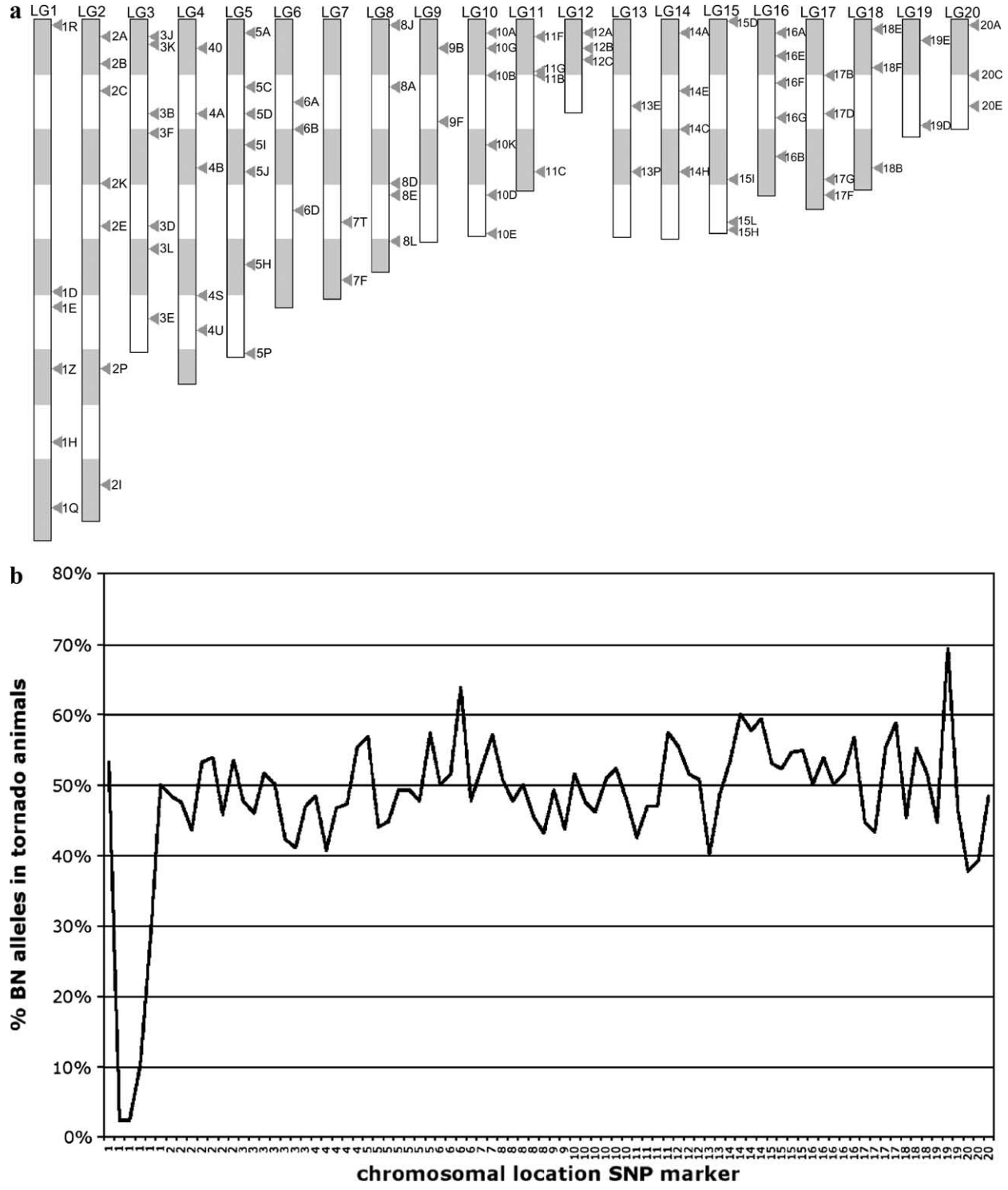

FIGURE 2.—SNP-based mapping of the tornado mutation. (a) Distribution on the rat physical map of the 84 verified SNP markers used for mapping the tornado mutation. SNPs were selected from equally sized genomic segments (represented in alternating open and shaded bars). The mapping cross showed that the mutation is inherited in a normal autosomal recessive manner, which made it unnecessary to include markers on the X chromosome. (b) Representation of linkage of the mutant phenotype to the central region of chromosome 1. The polymorphic SNP markers are plotted on the *x*-axis ordered by chromosome location (the numbers on the bottom represent the chromosomes). The graph shows the percentage of BN alleles, calculated from 67 genotyped tornado animals obtained from the mapping cross. The tornado mutation was introduced in the Wistar background.

TABLE 1

Candidate deafness genes mapping to rat chromosome 1

Locus	Gene	Human	Mouse	Rat	Reference
DFNA10	*EYA4*	6:133.5	10:22.8	1:22.8	Wayne *et al.* (2001)
DFNB2	*MYO7A*	11:76.6	7:86.5	1:155.4	Liu *et al.* (1998); Weil *et al.* (1995)
DFNB7/11	*TMC1*	9:70.8	19:20.1	1:224	Kurima *et al.* 2002
DFNB18	*USH1C*	11	7:34.8	1:96.8	Ahmed *et al.* 2002; Ouyang *et al.* (2002)
DFNB22	*OTOA*	16	7:109.4	1:180.1	Zwaenepoel *et al.* (2002)

Candidate deafness genes that map to rat chromosome 1 were selected from Hereditary Hearing Loss Homepage (http://www.uia.ac.be/dnalab/hhh/). Albino is located on chromosome 1 at 143.7 Mbp. Closest to albino is *Myo7a* in all three species. Chromosomal locations are in accordance with Ensembl Rat Genome Build release version 3.1.

from which candidate SNPs (Guryev *et al.* 2004; http://cascad.niob.knaw.nl) were selected. Although some candidate SNPs could be selected on the basis of Wistar mRNA data *vs.* Brown Norway whole genome shotgun (WGS) sequencing data, the majority of the candidate SNPs were mined from Sprague Dawley EST data *vs.* Brown Norway WGS data. All candidate SNPs were tested in the six founders (two Wistar males and four BN females) of the mapping cross, resulting in a final SNP panel containing 84 verified SNPs distributed over 67 different bins (Figure 2a).

A total of 67 tornado F_2 animals (34 from the initial mapping cross and 33 from later crosses) were genotyped for these SNPs (supplementary Figure S1 at http://www.genetics.org/supplemental/), confirming strong linkage to the central region of chromosome 1, where the albino locus also is located (Figure 2b). The tornado mutation localizes between markers rs8156543 and rs8173521 (dbSNP: http://www.ncbi.nlm.nih.gov/SNP/). With three crossing overs in 65 animals between rs8173521 and the tornado mutation, the estimated genetic distance is ~2.3 cM proximal to rs8173521.

Identification of the mutation by candidate gene approach: To identify candidate genes in the remaining genomic interval, we mapped the orthologs of known human and mouse deafness genes on the rat genome (Table 1). Five human genes were found to have orthologs on rat chromosome 1, with *Myo7a*, encoding an unconventional myosin, closest to the albino gene and the rs8173521 SNP marker in the rat. Resequencing all 47 coding exons of *Myo7a* (Ensembl ID: ENSRNOT00000019053; Figure 3a) revealed an A-to-T transversion (position 362) that completely segregates with the tornado phenotype in all crosses (Figure 3b). This muta-

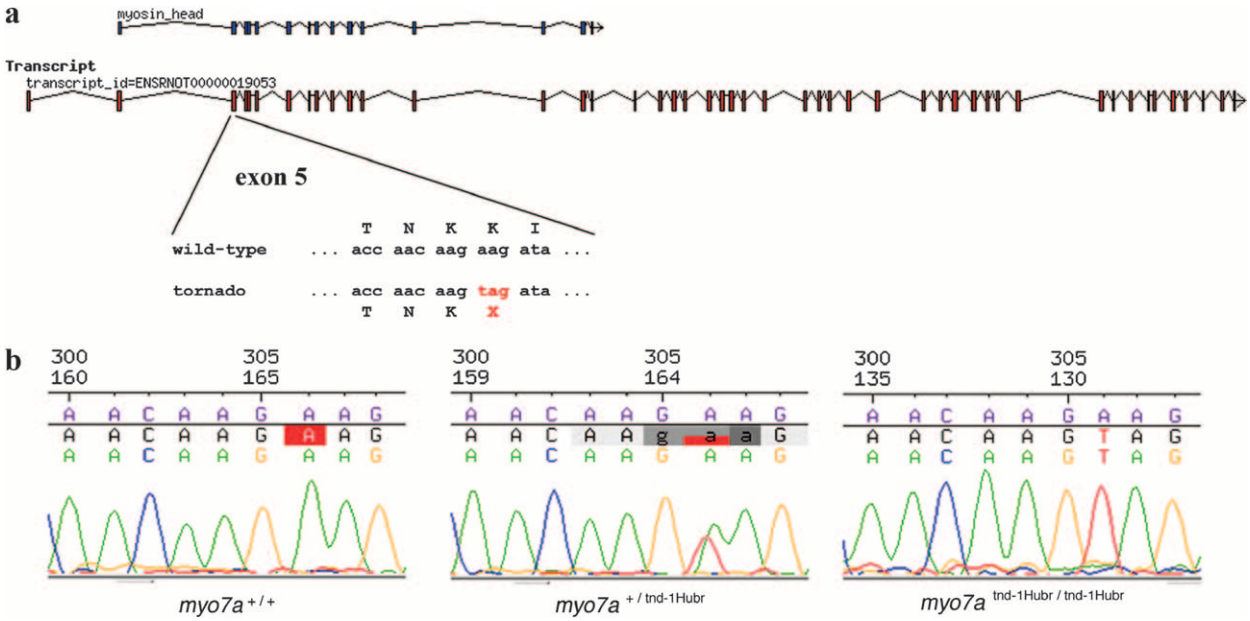

Figure 3.—The tornado phenotype is caused by a premature stopcodon in *Myo7a*. (a) Schematic organization of *Myo7a* in the rat and the position and context of the identified tornado mutation (*Myo7a*$^{tnd\text{-}1Hubr}$). The exons encoding the myosin head are indicated at the top of the graph. (b) Sequence traces of the mutated position in exon 5 of a homozygous wild-type (top), heterozygous (middle), and mutant (bottom) animal.

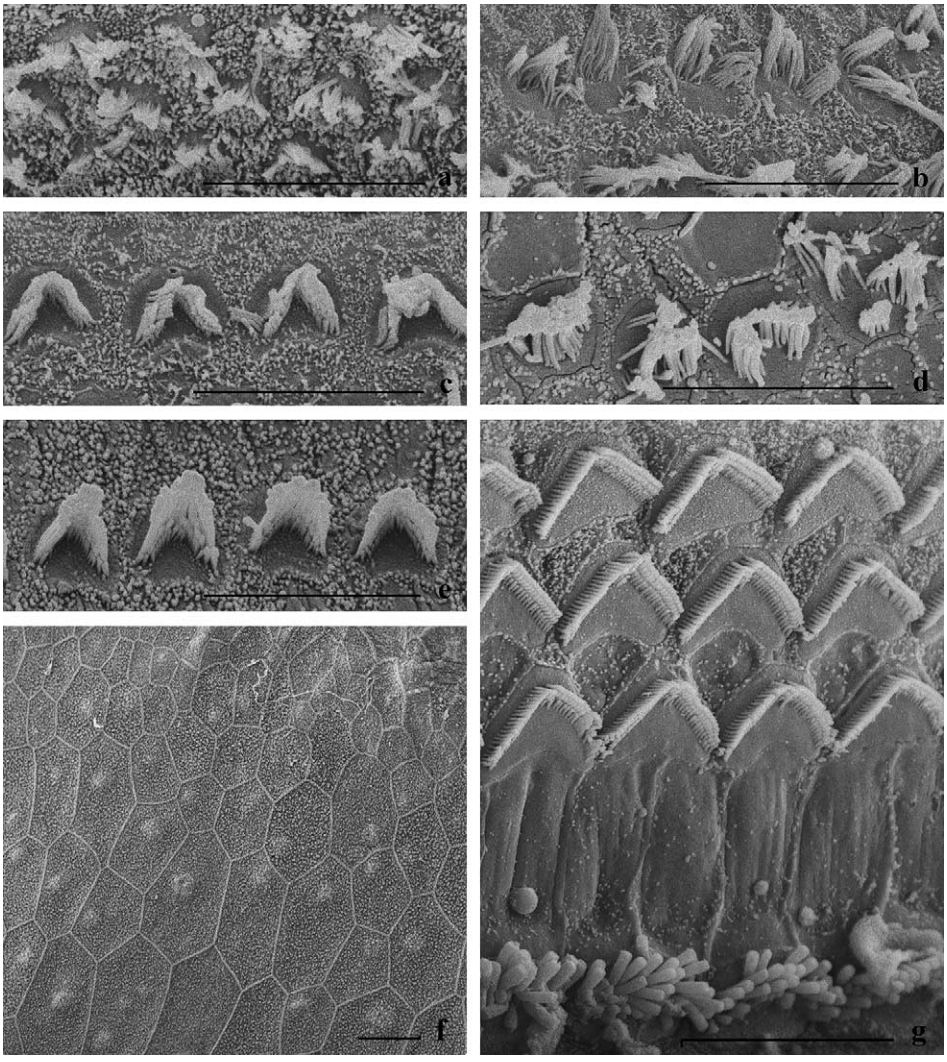

FIGURE 4.—Degeneration of the organ of Corti in tornado rats. SEM micrographs of the surface of the organ of Corti of tornado animals (*Myo7a*$^{tnd\text{-}1Hubr/tnd\text{-}1Hubr}$: a, b, d, and f and nonmutant littermates (*Myo7a*$^{tnd\text{-}1Hubr/+}$ or *Myo7a*$^{+/+}$: c, e, and g) at 6 days (a), 10 days (b and c), 20 days (d and e), and 13 weeks (f and g) of age. At 6 days of age, the outer hair cell stereocilia are already disorganized and fused (a) and degenerate progressively (b, d, and f) even on the inner hair cells (f). Eventually, an irregular epithelium remains in the organ of Corti region (f). Bars, 10 μm.

tion (*Myo7a*$^{tnd\text{-}1Hubr}$) introduces a premature stopcodon in exon 5 in the middle of the myosin head encoding sequence and thereby most likely results in a complete loss of function of the gene. Humans carrying mutations in *MYO7A* are known to suffer from Usher syndrome type IB, which is characterized by a profound congenital sensorineural hearing loss, constant vestibular dysfunction, and prepubertal onset of retinitis pigmentosa (WEIL *et al.* 1995). Most human disease-causing mutations, including premature stopcodons, deletions, and missense mutations, are located in the amino-terminal end of the motor domain of the protein. The first alleles of the shaker-1 mice that were cloned were found to be two missense mutations and a splice acceptor site mutation in the region encoding the myosin head of *Myo7a* (GIBSON *et al.* 1995).

Deafness and stereocilia disorganization in the tornado mutant: Scanning electron microscopy (SEM) on neuroepithelium of dissected cochlea, *i.e.*, of the upper surface of the hair cells of the organ of Corti, was used to investigate the cause of deafness. Normally, development of rat inner ear microanatomy and physiology leading to hearing starts around postnatal day 4 or 5 and hearing maturation is completed around postnatal day 20 (PUJOL *et al.* 1998). In the mutant rats, we observed disorganization, destruction, and fusing of the hair cell stereocilia, which was most pronounced on the outer hair cells, as early as 6 days after birth (Figure 4a). The hair cell stereocilia bundles degenerate progressively over a short time (Figure 4, b and d; controls are Figure 4, c and e, respectively), and in adult mutant rats no stereocilia can be detected on the outer or the inner hair cells (Figure 4f; control is Figure 4g). An irregular epithelium remains in the organ of Corti region (Figure 4f). In addition, the stereocilia degeneration progresses from the basal to the apical turn throughout the neuroepithelium of the cochlea (data not shown), suggesting complete deafness over the whole audible frequency range.

Air conducted ABR can be recorded as early as postnatal days 7–8 (GEAL-DOR *et al.* 1993). We explored ABR measurements on tornado and wild-type rats of 10 days and 4 weeks of age. The wild-type rats of 4 weeks of age displayed normal ABR patterns, with a detectable −7 dB

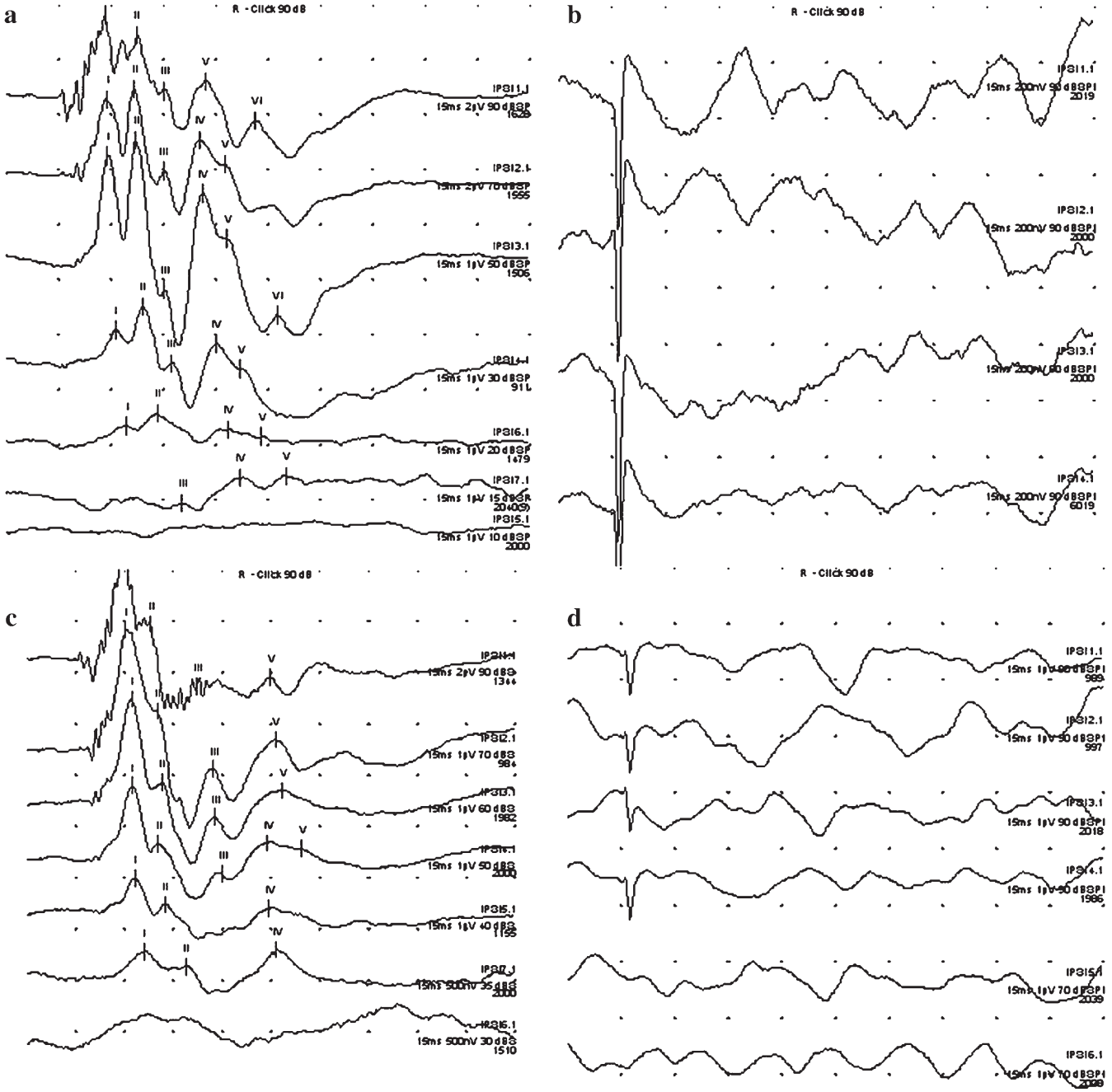

FIGURE 5.—Profound deafness in tornado rats. Typical auditory brain-stem responses from mutant tornado animals (*Myo7a*$^{tnd\text{-}1Hubr/tnd\text{-}1Hubr}$) and wild-type heterozygous littermates (*Myo7a*$^{tnd\text{-}1Hubr/+}$). (a) Four weeks of age, wild type; (b) 4 weeks of age, mutant; (c) 10 days of age, wild type; (d) 10 days of age, mutant. Horizontal axis: time window of 15 msec (1.5 msec/division); vertical axis: amplitude in microvolts. Stimulus onset at 1.5 msec. (Left, a and c) Good brain-stem responses obtained at different stimulation levels according to standard audiometrical descending top-down procedures until the level that no reproducible responses are recognized (*i.e.*, auditory threshold); (right, b and d) all responses reveal no reproducible brain-stem responses at a maximum stimulation level of 83 dB (SPL), including soundfield correction.

soundfield corrected threshold at 8 dB (SPL) ($n = 1$) (Figure 5a). In the mutant animals, no reproducible responses were observed at 83 dB (SPL) ($n = 2$) (Figure 5b). Wild-type juvenile rats of 10 days of age showed click-evoked responses between 18 and 43 dB (SPL) threshold level ($n = 4$) (Figure 5c: example of an auditory brain-stem threshold at 28 dB), but mutant littermates failed to show any reproducible click responses with settings up to 83 dB (SPL) ($n = 1$) (Figure 5d). Combining the observations of onset of stereocilia disorganization and no detectable responses to 83 dB click stimuli at 6 days of age and the severe stereocilia de-

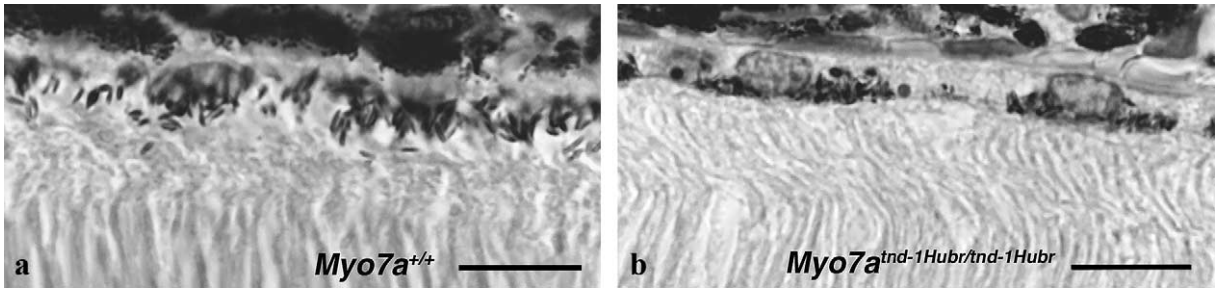

FIGURE 6.—Melanosome migration defect in tornado rats. Histological staining (hematoxylin/eosin) of the eyes of pigmented nonmutant (a) and tornado (b) animals, revealing the absence of melanosomes in the apical processes of the retinal pigment epithelium. Bars, 10 μm.

generation at 10 days of age, we conclude that tornado rats are most likely to be completely deaf throughout their life.

Eye phenotype: Prepubertal onset of blindness in USH1B patients is caused by degeneration of the retina (retinitis pigmentosa). The transport of opsin to the outer segment of photoreceptor cells seems especially critical for viability of these cells (MARSZALEK *et al.* 2000). It has been suggested that Myo7A coparticipates in opsin transport (LIU *et al.* 1999), but it still remains unclear how deficiency of functional Myo7A causes retinal degeneration in human patients. Moreover, for mice lacking functional Myo7A, retinal degeneration has never been diagnosed. Currently, however, two retinal phenotypes have been identified by microscopy in mice. First, LIU *et al.* (1998) found the absence of melanosomes in apical processes of the retinal pigment epithelium in Myo7A-deficient mice (LIU *et al.* 1998). The second mutant phenotype is a slower rate of photoreceptive disk membrane renewal in the outer segments (LIU *et al.* 1999), caused by perturbed phagocytosis of disk membranes (GIBBS *et al.* 2003).

Similar to LIU *et al.* (1998), we found an absence of melanosomes in the apical processes of retinal pigment epithelium in a tornado background at 5 weeks of age (Figure 6a; control is Figure 6b). However, both pigmented and albino tornado rats did not show any signs of retinal degeneration at 20 weeks of age (data not shown).

DISCUSSION

We initially established ENU mutagenesis conditions for the rat in setting up gene-driven knockout technology using target-selected mutagenesis (SMITS *et al.* 2004). However, the same F_1 animals are also suited for forward genetic, phenotype-driven approaches. Indeed, several phenotypes caused by dominant mutations were readily identified in our experiments (SMITS *et al.* 2004) as well as by others (ZAN *et al.* 2003). Gould and colleagues (ZAN *et al.* 2003) identified 74 visually aberrant mutants in a screen for dominant phenotypes in nearly 5000 F_1 progeny from ENU-treated Sprague Dawley rats. About half of them were found to be fertile and to inherit the phenotype. Here, we describe a small-scale study on recessive phenotypes after ENU mutagenesis in the rat and the subsequent cloning of the mutated gene using a novel SNP mapping panel. Although the SNP mapping panel is of relatively low density and specifically designed for mapping crosses between Wistar and Brown Norway, it can easily be adapted or expanded with more SNPs, since public databases now harbor >50,000 candidate and validated SNPs.

The genome scan carried out using our SNP panel pointed toward a region on chromosome 1 containing *Myo7a*, the ortholog of the human Usher syndrome type 1B gene. Resequencing of the coding region of this gene in the tornado rat identified a nonsense mutation in the middle of the core domain, the myosin head. Human patients with Usher syndrome type 1B, also harboring mutations in the myosin head, suffer from profound congenital deafness (WEIL *et al.* 1995). Shaker-1, the mouse model for Usher syndrome type 1B, also displays severe congenital hearing impairment due to typical neuroepithelial-type cochlear defects (GIBSON *et al.* 1995). In 1998, SELF *et al.* (1998) described the correlation between the nature of the mutation, the severity of stereocilia disorganization, and electrophysiological response in three different alleles of *Myo7a* in the mouse. The most severe disruption of development of the stereocilia was observed in $Myo7a^{816SB}$, a mutant lacking 10-amino-acid residues of the core of the motor head. These animals showed complete absence of stimulus-related cochlear potentials. Mice with a relatively mild shaker-1 phenotype ($Myo7a^{6J}$) already show prenatal disorganization of stereocilia in the organ of Corti, whereas the microvilli at the upper surface of the hair cell, from which the stereocilia develop, are unaffected at embryonic day 16.5. The tornado rat allele described here ($Myo7a^{tnd\text{-}1Hubr}$) is likely to resemble the severe mouse and the common human alleles, as the premature stop-codon in the beginning of the gene is expected to result in complete loss of gene function. Indeed, in the tornado rat, stereocilia disorganization is obvious at 6 days

of age and results in complete degeneration of cochlear hair cells within 1 month after birth. Furthermore, measurements of brain-stem responses to auditory stimuli suggest that tornado animals are deaf throughout life.

Taken together, the identification of the first rat model for Usher syndrome type 1B may contribute to the further understanding of the molecular mechanisms underlying Usher syndrome type IB and healthy and diseased inner ear and eye function in general. A major advantage of a rat model over a mouse model for studying inner ear function may be the size and accessibility of the organism, for example, for cochlear implant studies (Vischer *et al.* 1997). Finally, the *Myo7a*$^{tnd\text{-}1Hubr}$ mutant described here is the first rat model induced by ENU mutagenesis that is cloned by forward genetics, providing proof of principle for systematic forward genetics in the rat. Large-scale phenotype-driven screens in the rat have the potency to result in important new insights in the function of genes in the development of complex disease and higher brain functions, for which the rat currently is the best-suited model organism.

We thank J. Korving for histological sections on retinas and J. Curfs for help with the ABR measurements. This work was supported by the Dutch Ministry of Economic Affairs through the Innovation Oriented Research Program on Genomics and NV Organon.

LITERATURE CITED

Ahmed, Z. M., T. N. Smith, S. Riazuddin, T. Makishima, M. Ghosh *et al.*, 2002 Nonsyndromic recessive deafness DFNB18 and Usher syndrome type IC are allelic mutations of USHIC. Hum. Genet. **110:** 527–531.

Alagramam, K. N., C. L. Murcia, H. Y. Kwon, K. S. Pawlowski, C. G. Wright *et al.*, 2001 The mouse Ames waltzer hearing-loss mutant is caused by mutation of Pcdh15, a novel protocadherin gene. Nat. Genet. **27:** 99–102.

Bockamp, E., M. Maringer, C. Spangenberg, S. Fees, S. Fraser *et al.*, 2002 Of mice and models: improved animal models for biomedical research. Physiol. Genomics **11:** 115–132.

Brown, S. D., and R. Balling, 2001 Systematic approaches to mouse mutagenesis. Curr. Opin. Genet. Dev. **11:** 268–273.

Brown, S. D., and P. M. Nolan, 1998 Mouse mutagenesis-systematic studies of mammalian gene function. Hum. Mol. Genet. **7:** 1627–1633.

Canzian, F., 1997 Phylogenetics of the laboratory rat Rattus norvegicus. Genome Res. **7:** 262–267.

Chwalisz, W. T., B. U. Koelsch, A. Kindler-Rohrborn, H. J. Hedrich and D. Wedekind, 2003 The circling behavior of the deaf-blind LEW-ci2 rat is linked to a segment of RNO10 containing Myo15 and Kcnj12. Mamm. Genome **14:** 620–627.

Cox, R. D., and S. D. Brown, 2003 Rodent models of genetic disease. Curr. Opin. Genet. Dev. **13:** 278–283.

Geal-Dor, M., S. Freeman, G. Li and H. Sohmer, 1993 Development of hearing in neonatal rats: air and bone conducted ABR thresholds. Hear. Res. **69:** 236–242.

Gibbs, D., J. Kitamoto and D. S. Williams, 2003 Abnormal phagocytosis by retinal pigmented epithelium that lacks myosin VIIa, the Usher syndrome 1B protein. Proc. Natl. Acad. Sci. USA **100:** 6481–6486.

Gibbs, R. A., G. M. Weinstock, M. L. Metzker, D. M. Muzny, E. J. Sodergren *et al.*, 2004 Genome sequence of the brown Norway rat yields insights into mammalian evolution. Nature **428:** 493–521.

Gibson, F., J. Walsh, P. Mburu, A. Varela, K. A. Brown *et al.*, 1995 A type VII myosin encoded by the mouse deafness gene shaker-1. Nature **374:** 62–64.

Greenhouse, D. D., M. W. F. Festing, S. Hasan and A. L. Cohen, 1990 Catalog of inbred strains of rats, pp. 411–480 in *Genetic Monitoring of Inbred Strains of Rats: A Manual on Colony Management, Basic Monitoring Techniques, and Genetic Variants of the Laboratory Rat*, edited by H. J. Hedrich and M. Adams. Gustav Fisher Verlag, Stuttgart, Germany.

Guryev, V., E. Berezikov, R. Malik, R. H. Plasterk and E. Cuppen, 2004 Single nucleotide polymorphisms associated with rat expressed sequences. Genome Res. **14:** 1438–1443.

Hedrich, H. J., 2000 History, strains, and models, pp. 3–16 in *The Handbook of Experimental Animals: The Laboratory Rat*, edited by G. J. Krinke. Academic Press, San Diego.

Jacob, H. J., and A. E. Kwitek, 2002 Rat genetics: attaching physiology and pharmacology to the genome. Nat. Rev. Genet. **3:** 33–42.

Jacob, H. J., A. Pettersson, D. Wilson, Y. Mao, A. Lernmark *et al.*, 1992 Genetic dissection of autoimmune type I diabetes in the BB rat. Nat. Genet. **2:** 56–60.

Jewett, D. L., and J. S. Williston, 1971 Auditory-evoked far fields averaged from the scalp of humans. Brain **94:** 681–696.

Keays, D. A., and P. M. Nolan, 2003 N-ethyl-N-nitrosourea mouse mutants in the dissection of behavioural and psychiatric disorders. Eur. J. Pharmacol. **480:** 205–217.

Kuramoto, T., M. Kuwamura and T. Serikawa, 2004 Rat neurological mutations cerebellar vermis defect and hobble are caused by mutations in the netrin-1 receptor gene Unc5h3. Brain Res. Mol. Brain Res. **122:** 103–108.

Kurima, K., L. M. Peters, Y. Yang, S. Riazuddin, Z. M. Ahmed *et al.*, 2002 Dominant and recessive deafness caused by mutations of a novel gene, TMC1, required for cochlear hair-cell function. Nat. Genet. **30:** 277–284.

Liu, X., B. Ondek and D. S. Williams, 1998 Mutant myosin VIIa causes defective melanosome distribution in the RPE of shaker-1 mice. Nat. Genet. **19:** 117–118.

Liu, X., I. P. Udovichenko, S. D. Brown, K. P. Steel and D. S. Williams, 1999 Myosin VIIa participates in opsin transport through the photoreceptor cilium. J. Neurosci. **19:** 6267–6274.

Marszalek, J. R., X. Liu, E. A. Roberts, D. Chui, J. D. Marth *et al.*, 2000 Genetic evidence for selective transport of opsin and arrestin by kinesin-II in mammalian photoreceptors. Cell **102:** 175–187.

Mburu, P., M. Mustapha, A. Varela, D. Weil, A. El-Amraoui *et al.*, 2003 Defects in whirlin, a PDZ domain molecule involved in stereocilia elongation, cause deafness in the whirler mouse and families with DFNB31. Nat. Genet. **34:** 421–428.

Nickerson, D. A., V. O. Tobe and S. L. Taylor, 1997 PolyPhred: automating the detection and genotyping of single nucleotide substitutions using fluorescence-based resequencing. Nucleic Acids Res. **25:** 2745–2751.

O'Brien, T. P., and W. N. Frankel, 2004 Moving forward with chemical mutagenesis in the mouse. J. Physiol. **554:** 13–21.

Ouyang, X. M., X. J. Xia, E. Verpy, L. L. Du, A. Pandya *et al.*, 2002 Mutations in the alternatively spliced exons of USH1C cause nonsyndromic recessive deafness. Hum. Genet. **111:** 26–30.

Pujol, R., M. Lavigne-Rebillard and M. Lenoir, 1998 Development of sensory and neural structures in the mammalian cochlea, pp. 146–192 in *Development of the Auditory System*, edited by E. W. Rubel, A. N. Popper and R. R. Fay. Springer-Verlag, New York.

Rapp, J. P., 2000 Genetic analysis of inherited hypertension in the rat. Physiol. Rev. **80:** 135–172.

Rozen, S., and H. Skaletsky, 2000 Primer3 on the WWW for general users and for biologist programmers. Methods Mol. Biol. **132:** 365–386.

Self, T., M. Mahony, J. Fleming, J. Walsh, S. D. Brown *et al.*, 1998 Shaker-1 mutations reveal roles for myosin VIIA in both development and function of cochlear hair cells. Development **125:** 557–566.

Shepel, L. A., H. Lan, J. D. Haag, G. M. Brasic, M. E. Gheen *et al.*, 1998 Genetic identification of multiple loci that control breast cancer susceptibility in the rat. Genetics **149:** 289–299.

Smits, B. M., J. Mudde, R. H. Plasterk and E. Cuppen, 2004 Target-selected mutagenesis of the rat. Genomics **83:** 332–334.

Thomas, M. A., C. F. Chen, M. I. Jensen-Seaman, P. J. Tonellato and S. N. Twigger, 2003 Phylogenetics of rat inbred strains. Mamm. Genome **14:** 61–64.

van der Weyden, L., D. J. Adams and A. Bradley, 2002 Tools for targeted manipulation of the mouse genome. Physiol. Genomics **11:** 133–164.

Vischer, M., A. Haenggeli, J. Zhang, M. Pelizzone, R. Hausler

et al., 1997 Effect of high-frequency electrical stimulation of the auditory nerve in an animal model of cochlear implants. Am. J. Otol. **18:** S27–S29.

Wang, A., Y. Liang, R. A. Fridell, F. J. Probst, E. R. Wilcox *et al.*, 1998 Association of unconventional myosin MYO15 mutations with human nonsyndromic deafness DFNB3. Science **280:** 1447–1451.

Wayne, S., N. G. Robertson, F. DeClau, N. Chen, K. Verhoeven *et al.*, 2001 Mutations in the transcriptional activator EYA4 cause late-onset deafness at the DFNA10 locus. Hum. Mol. Genet. **10:** 195–200.

Weil, D., S. Blanchard, J. Kaplan, P. Guilford, F. Gibson *et al.*, 1995 Defective myosin VIIA gene responsible for Usher syndrome type 1B. Nature **374:** 60–61.

Wilson, S. M., D. B. Householder, V. Coppola, L. Tessarollo, B. Fritzsch *et al.*, 2001 Mutations in Cdh23 cause nonsyndromic hearing loss in waltzer mice. Genomics **74:** 228–233.

Zan, Y., J. D. Haag, K. S. Chen, L. A. Shepel, D. Wigington *et al.*, 2003 Production of knockout rats using ENU mutagenesis and a yeast-based screening assay. Nat. Biotechnol. **21:** 645–651.

Zimdahl, H., G. Nyakatura, P. Brandt, H. Schulz, O. Hummel *et al.*, 2004 A SNP map of the rat genome generated from cDNA sequences. Science **303:** 807.

Zwaenepoel, I., M. Mustapha, M. Leibovici, E. Verpy, R. Goodyear *et al.*, 2002 Otoancorin, an inner ear protein restricted to the interface between the apical surface of sensory epithelia and their overlying acellular gels, is defective in autosomal recessive deafness DFNB22. Proc. Natl. Acad. Sci. USA **99:** 6240–6245.

Communicating editor: M. Justice